Research Square

Preprints are preliminary reports that have not undergone peer review.
They should not be considered conclusive, used to inform clinical practice,
or referenced by the media as validated information.

A Quantum-Classical Hybrid Framework for Optimal Energy Storage Systems Planning

Md Shamim Hasan

hasanm1@ornl.gov

Oak Ridge National Laboratory

Willie Aboumrad

IonQ (United States)

Phani R.V. Marthi

Oak Ridge National Laboratory

Evgeny Epifanovsky

IonQ (United States)

George Siopsis

IonQ (United States)

Martin Roetteler

IonQ (United States)

Suman Debnath

Oak Ridge National Laboratory

Article

Keywords: Energy storage systems, optimal siting and sizing, substation power-flow deviation, hybrid quantum–classical optimization, QUBO, convex optimization

Posted Date: June 11th, 2026

DOI: https://doi.org/10.21203/rs.3.rs-9557230/v1

License: This work is licensed under a Creative Commons Attribution 4.0 International License.
Read Full License

Additional Declarations: No competing interests reported.

Version of Record: A version of this preprint was published at Scientific Reports on July 18th, 2026. See the published version at https://doi.org/10.1038/s41598-026-62843-2.

A Quantum-Classical Hybrid Framework for Optimal Energy Storage Systems Planning

Md Shamim Hasan[1*†], Willie Aboumrad[2†], Phani R. V. Marthi[1*], Evgeny Epifanovsky[2], George Siopsis[3], Martin Roetteler[2], Suman Debnath[1]

[1*]Power System Resilience, Oak Ridge National Laboratory, 1 Bethel Valley Road, Oak Ridge, TN, USA.
[2]IonQ Inc., College Park, MD, USA.
[3] IonQ Inc., Chattanooga, TN, USA.

*Corresponding author(s). E-mail(s): hasanm1@ornl.gov; marthip@ornl.gov;
Contributing authors: aboumrad@ionq.co; epifanovsky@ionq.co; george.siopsis@ionq.co; martin.roetteler@ionq.co; debnaths@ornl.gov;
†These authors contributed equally to this work.

Abstract

The extensive deployment of power-electronics introduce spatial-temporal variability that can degrade voltage quality and operational reliability. Energy storage systems (ESS) can mitigate these effects through fast active and reactive power support, but their value is contingent on coordinated siting and sizing. Integrated formulations that minimize voltage deviations, reduce substation power-flow variability, and account for installation costs typically yield in large-scale mixed-integer optimization problems that are computationally burdensome for classical solvers and may yet not lead to the most optimum solution. To address these challenges, this paper proposes a two-stage hybrid quantum–classical planning framework that separates binary siting from continuous sizing and operation. In Stage I, the siting problem is reformulated as a Quadratic Unconstrained Binary Optimization model and solved via a hybrid quantum workflow. Acting as a "quantum sieve," stochastic sampling generates a diverse set of candidate site combinations that classical single-point methods can overlook. In Stage II, selected site sets are evaluated using a classical convex solver (SOCP) to compute optimal ESS capacities and operating setpoints subject to network constraints, ensuring physical feasibility. Experiments on IonQ Forte hardware show grid-standard accuracy with industry-standard classical

solvers. Although current hardware latencies limit performance in the NISQ era, the paper outlines scaling pathways and discusses key practical hurdles, including state-preparation overlap and higher-order cost couplings.

Keywords: Energy storage systems, optimal siting and sizing, substation power-flow deviation, hybrid quantum–classical optimization, QUBO, convex optimization.

1 Introduction

Modern transmission–distribution networks are increasingly dominated by power-electronics, which introduce fast, state-dependent dynamics and spatial–temporal variability in net injections. Grid-connected energy storage systems (ESS) can mitigate these effects by delivering fast active/reactive power support for voltage regulation, congestion relief, and energy-flow smoothing [1, 2] by storing excess electricity generated by power electronic based generations and releasing it when needed [3]. However, these benefits are highly contingent on the location and size of the storage units [4]. Poor siting can necessitate oversized devices to meet voltage/thermal constraints, whereas "minimum-capacity" placements may still underperform in loss reduction or voltage control, motivating multi-criteria planning (e.g., voltage deviation, feeder/substation loading, and cost) rather than single-objective heuristics [5–8]. Consequently, optimal ESS siting–sizing is now viewed as a core planning task for distribution system operators (DSOs) and transmission system operators (TSOs), yet realistic formulations remain challenging when jointly considering operational constraints, investment, and energy costs over planning horizons, and multiple scenarios/uncertainties—often leading to large-scale mixed-integer optimization problems with nontrivial computational burden [8, 9].

Despite extensive literature on ESS planning, the combined siting–sizing problem is inherently challenging because it is a mixed-integer program: siting introduces binary decision variables (install or not), while sizing and operation remain continuous. Classical mixed-integer formulations can suffer from poor scalability, sensitivity to relaxation gaps, and feasibility issues when network constraints, multi-objective metrics, and operational coupling are modeled with high fidelity [9]. Quadratic unconstrained binary optimization (QUBO) is attractive here because it provides a standard way to represent binary decisions using a quadratic objective with penalties that absorb constraints, enabling direct mapping to Ising/QUBO solvers and annealing-based hardware [10, 11]. This is precisely the computational "bridge" exploited in recent power system studies that recast combinatorial network problems into QUBO form and solve them using quantum or quantum–classical hybrid approaches [12–14], while broader reviews also emphasize QUBO-mapping and hybrid paradigms as practical near-term pathways for grid optimization under noisy intermediate-scale quantum (NISQ) constraints [15]. In this context, separating (i) the binary siting stage as a QUBO and (ii) the continuous sizing/dispatch stage as a convex classical program provides a principled route to reduce infeasibility/scaling issues, and improves tractability

while utilizing quantum hardware where it is naturally suited— discrete search over large combinatorial spaces.

Most research has been conducted on determining the optimal location and sizing of ESS in distribution networks to address key challenges, such as intermittency, voltage deviations, and cost efficiency, are limited to classical optimization approach [3, 16]. One of the early studies on optimal sizing and placement of ESS is presented in [17] where the minimum required capacity and optimal location is determined by optimizing the exchange of both active and reactive power between the ESS and its grid-tied inverter (GTI), taking into account the network topology and the system's R/X ratios. However, the approach may face scalability challenges due to the required inversion of the equivalent impedance matrix ($Z_{eq_{kj}}$). In [18], ESS was optimally placed in an IEEE 33-bus system to minimize the net present value of energy loss costs, using the Grey Wolf Optimization (GWO) algorithm and comparing it with a genetic algorithm (GA), particle swarm optimization (PSO), symbiotic organisms search algorithm (SOS), and firefly algorithm (FA). Convex optimization was applied in [19] to find the optimal size of ESS in an off-grid microgrid, aiming to minimize total costs including fuel, installation, operation, and maintenance. A coyote optimization algorithm was proposed in [20] for locating and sizing of one or two ESS units, respectively, in a 48-bus system, with comparisons to PSO, and FA. In [21], ESS was integrated in a 33-bus system to reduce power losses. ESS sizing optimization was presented in [22], focusing on reactive power support and voltage profile improvement in a 36-bus system using Genetic Algorithm (GA). In addition, [23] employed the Grasshopper Optimization (GO) method to optimize ESS capacity and placement, reducing line loss and voltage profile improvement. However, these approaches [17, 18, 20–23] are heuristic and do not provide feasibility or optimality guarantees [24]. Moreover, the computational burden implied by these approaches becomes impractical as we scale to industrial problem sizes. In addition, these studies [17–23] focus on single-objective optimization and fail to consider trade-offs amongst competing priorities.

Several studies have adopted multi-objective optimization approaches to determine the optimal placement and sizing of ESS. In [2], a multi-objective framework was proposed for shared ESS deployment in urban energy communities, aiming to balance economic, technical, and environmental performance by minimizing the net present value of installation and maximizing energy self-efficiency. However, this work did not address voltage deviation. The study in [25] considered minimizing total costs and voltage deviations, but did not look into substation power flow deviation. In [26], a multi-objective model was developed to minimize bus voltage fluctuation, energy storage capacity, and substation power deviation with a 24-hours 24-steps problem, but it did not consider system cost. These studies also employed heuristic algorithms, such as, GA, Peafowl Optimization Algorithm, and Particle Swamp Optimization to solve their respective optimization problems. While heuristics are flexible and widely used, they are typically problem-specific, computationally expensive, and fail to achieve global optimality [24]. In contrast, convex and quadratic optimization methods are generally preferred for their well defined mathematical structure, superior convergence properties, and scalability across larger systems.

Recent literature has begun to demonstrate that quantum and quantum-inspired optimization can address the combinatorial bottlenecks arising in power-system operation and planning (e.g., OPF with discrete controls, unit commitment, switching/topology decisions, and related mixed-integer variants) [27]. Tutorial/review articles targeting the power-systems community summarize three dominant directions: gate-based algorithms (e.g., QAOA/VQE-style approaches), annealing-based methods (quantum annealing / adiabatic optimization), and quantum-inspired solvers (digital annealers and hybrid classical–quantum workflows), while also emphasizing practical near-term use cases and limitations under NISQ-era constraints [15]. A notable example in grid optimization is the work on annealing-based quantum computing for combinatorial OPF proposed in [12], which reformulates discrete OPF variants into an annealer-suitable model to explore large binary decision spaces. Beyond OPF, a QUBO/Ising-based power-flow analysis approach was evaluated on both quantum and digital annealers, demonstrating that even foundational nonlinear grid computations can be recast as discrete optimization problems [14]. For operations problems, recent studies propose hybrid decomposition/coordination frameworks that embed quantum annealing as a sub-solver for unit commitment, and benchmarking papers evaluate hybrid quantum-annealing solvers on realistic UC instances, highlighting where quantum/hybrid approaches may help and where classical methods remain superior [28, 29]. Collectively, these works motivate the use of QUBO/Ising formulations as a "common language" that maps binary grid decisions to emerging quantum/hybrid solvers for solving binary nonlinear optimization problem, thereby opening a pathway for early deployments in planning problems such as ESS siting (binary) coupled with classical sizing/dispatch (continuous).

Based on the preceding discussion, it is evident that existing research lacks a comprehensive approach to the optimal sizing and placement of ESS that simultaneously considers cost minimization, reduction in voltage deviation, and minimization of substation power flow. Furthermore, unlike prior works that either (a) rely on mixed-integer solvers with limited scalability or (b) optimize a single operational metric, the proposed framework produces multiple feasible ESS design candidates with explicit trade-offs among voltage quality, substation power variability, and cost. The main contributions of this paper are as follows:

- *Integrated ESS planning objective with grid-operational relevance*: A coordinated ESS planning model is formulated that combines minimization of (i) network voltage deviation, (ii) substation power-flow deviation, and (iii) installation and operational energy costs, bridging technical performance and economic practicality in a single planning workflow.
- *Two-stage decomposition that resolves the mixed-integer bottleneck*: A two-stage hybrid planning framework is developed that separates the binary siting decisions from continuous sizing/operation. The ESS siting task is casted as a QUBO and implement a hybrid quantum–classical solver, enabling the discrete combinatorial search to be performed on quantum hardware. Given the candidate sites from the QUBO stage, the multi-objective function is relaxed with Taylor series expansion and solved ESS sizing and operating setpoints using a convex optimization model

under network operating limits. This process avoids the infeasibility and scalability challenges commonly encountered in monolithic mixed-integer formulations.

- *Hardware-backed validation and solution*: Experimental results are provided using quantum hardware, showing that the quantum-enabled siting stage can provide distinct candidate site sets (solution diversity) compared to conventional classical approaches, which may return multiple equivalent optima or be sensitive to initialization/relaxations. This highlights the potential of quantum hardware to broaden the solution landscape for ESS planning. To the best of the authors' knowledge, this work represents one of the first practical demonstrations of quantum/hybrid optimization applied to joint ESS location and sizing in power system planning with explicit grid-performance and cost objectives.

The rest of the paper is organized as follows. Section 2 formally introduces the ESS placement and sizing problem as a nonconvex mixed-integer program (MIP) with non-linear constraints and how we relaxed it to form a fully convex problem. Section 3 details a two-step heuristic for solving ESS placement and sizing, and then Section 4 discusses optimization results. Section 5 addresses quantum scalability. Finally, we conclude with a few avenues for further research in Section 6.

2 Design problem formulation

Consider a power network $\mathcal{N} = (\mathcal{B}, \mathcal{L})$ where $\mathcal{B}$ denotes the set of buses and $\mathcal{L}$ denotes the set lines. We assume there is electric demand, also called load, at each bus. In addition, we assume certain buses can supply power, either because they act as the network's substation, or because they are equipped with an ESS. Without loss of generality, we label the buses in $\mathcal{B}$ by $i = 1, \ldots, M$, and we label the network substation $i = 1$. The aim of the ESS Design Problem (ESSDP) is to determine the optimal placement and sizing of a number of ESS units to satisfy the power demanded at each bus while minimizing voltage fluctuations across the buses, the active power drawn from the substation, and the total installation cost of the ESS units.

2.1 Objective

We formulate this problem as a multi-objective program with three primary objectives. Let $P^t_{g,i}$ and $Q^t_{g,i}$ denote the real and reactive power generated at bus i during time period t; correspondingly, $P^t_{d,i}$ and $Q^t_{d,i}$ denote the real and reactive power demanded at bus i during time period t. Furthermore, let U_i denote the complex voltage at bus i, and express it in polar form as $U_i = |U_i|(\cos\theta_i + \mathrm{i}\sin\theta_i)$. Here $\mathrm{i} = \sqrt{-1}$.

We follow power system analysis conventions and normalize the voltage magnitude against the initial substation voltage and express all voltage magnitudes in per unit (p.u.). Thus the nominal value is unity.

The voltage deviation and substation power deviation objectives are given by:

$$C_V(U) = \sum_{t\in\mathcal{T}} \sum_{i\in\mathcal{B}} \left(|U^t_i| - 1\right)^2, \quad \text{and} \tag{1}$$

$$C_S(P) = \sum_{t\in\mathcal{T}} \left|P^t_{g,1} - \overline{P}\right|, \tag{2}$$

with $\overline{P}$ denoting the average substation power. We model the installation cost of the ESS at bus i as a quadratic function of the system's energy storage capacity E_i. Thus the total installation cost is given by

$$C_B(E,s) = \sum_{i\in\mathcal{B}} s_i\big(a_i E_i^2 + b_i E_i + c_i\big), \tag{3}$$

with $s_i \in \{0,1\}$ denoting whether bus i is equipped with an ESS. The overall objective is to minimize the linear combination

$$\alpha C_V + \beta C_S + \gamma C_B, \tag{4}$$

for some $\alpha, \beta, \gamma > 0$.

Our multi-objective formulation reflects the complicated real-world trade-offs that arise in the deployment of ESS units to commercial networks; the problem constraints tie all the variables together, thereby creating complex Pareto fronts.

2.2 Constraints

For any given $s \in \{0,1\}^M$, the network $\mathcal{N}$ models a physical transmission network, so every feasible solution to the ESSDP must satisfy the constraints of an Optimal Power Flow (OPF) problem on $\mathcal{N}$ with the buses in $\{i \in \mathcal{B} \mid s_i = 1\}$ acting as generators. Thus, we begin by recalling an alternative formulation to the OPF problem in the so-called "rectangular form" [9, 30]. Let G_{ij} and B_{ij} denote the conductance and susceptance of each line $(i,j) \in \mathcal{L}$. Define $G_{ii} = g_{ii} - \sum_{j\neq i} G_{ij}$ and $B_{ii} = b_{ii} - \sum_{j\neq i} B_{ij}$, with g_{ii} and b_{ii} denoting the shunt conductance and shunt susceptance at bus $i \in \mathcal{B}$. The constraint set of the OPF problem at each time period $t \in \mathcal{T} = \{1,\dots,T\}$ is given as follows:

$$P^t_{g,i} - P^t_{d,i} = G_{ii}|U^t_i|^2 + \sum_{j\in\delta(i)} \big(G_{ij}C^t_{ij} - B_{ij}S^t_{ij}\big) \tag{5}$$

$$Q^t_{g,i} - Q^t_{d,i} = -B_{ii}|U^t_i|^2 + \sum_{j\in\delta(i)} \big(-B_{ij}C^t_{ij} - G_{ij}S^t_{ij}\big), \tag{6}$$

$$C^t_{ij} = |U^t_i||U^t_j|\cos(\theta_i - \theta_j), \quad (i,j)\in\mathcal{L}, \tag{7}$$

$$S^t_{ij} = |U^t_i||U^t_j|\sin(\theta_i - \theta_j), \quad (i,j)\in\mathcal{L}, \tag{8}$$

$$\underline{U_i} \le |U^t_i| \le \overline{U_i}, \qquad i\in\mathcal{B}, \tag{9}$$

$$s_i\cdot\underline{P_{g,i}} \le P^t_{g,i} \le s_i\cdot\overline{P_{g,i}}, \qquad i>1, \tag{10}$$

$$s_i\cdot\underline{Q_{g,i}} \le Q^t_{g,i} \le s_i\cdot\overline{Q_{g,i}}, \qquad i>1. \tag{11}$$

Constraints (5) and (6) represent the conservation of active and reactive power flows at each bus, at each time period; here $\delta(i)$ denotes the set of buses adjacent to bus i. The trigonometric terms in constraints (7) and (8) present a formidable obstacle in the solution of large-scale OPF problem instances; the convex relaxation used in this work serves as a workable alternative. Constraint (9) restricts the voltage magnitudes to be close to the initial substation voltage at all times; in both test cases considered here, $\underline{U_i} = 0.95$ and $\overline{U_i} = 1.05$ p.u. Constraints (10) and (11) limit the real and reactive power output by each ESS unit according to its physical capacity at every bus i for which $s_i = 1$, and they ensure no power is generated at a bus that's not equipped with an ESS, i.e., at buses for which $s_i = 0$.

The ESSDP imposes several additional constraints. For starters, the total power generated is required to meet the demand at each time period. In addition, to ensure practical feasibility, we require that each ESS unit installed has enough capacity to cover peak power output over the time horizon. Moreover, there are minimum and maximum capacity constraints for each ESS related to sunk costs and the physical space available at each bus location. Finally, we consider the case where at most N ESS units can be installed. In symbols, this means the ESSDP features the following additional constraints:

$$\sum_{i\in\mathcal{B}} P^t_{g,i} \geq \sum_{i\in\mathcal{B}} P^t_{d,i}, \qquad t \in \mathcal{T}, \tag{12}$$

$$E_i = \max_{t\in\mathcal{T}} |P^t_{g,i}|, \qquad i \in \mathcal{B}, \tag{13}$$

$$\underline{E_i} \leq E_i \leq \overline{E_i}, \qquad i \in \mathcal{B}, \tag{14}$$

$$\sum_{i\in\mathcal{B}} s_i \leq N \tag{15}$$

$$s_1 = 0. \tag{16}$$

All in all, we obtain the non-linear non-convex ESSDP MIP:

$$\begin{aligned} \text{minimize} \quad & (4) \\ \text{s.t.} \quad & (5) - (16). \end{aligned} \tag{17}$$

2.3 Convex Relaxation

Now we convert the non-linear mixed integer optimization problem to a discplined convex mixed integer optimization problem. As a stepping stone towards a convex relaxation, we follow [9] to obtain a formulation that produces the optimal power outputs for Problem (17) on a radial network. This reformulation results from the change of variables defined by $C^t_{ii} = |U^t_i|^2$ together with (7) and (8). Under this change of variables, constraint (9) becomes

$$\underline{U_i}^2 \leq C^t_{ii} \leq \overline{U_i}^2, \qquad i \in \mathcal{B},\, t \in \mathcal{T}. \tag{18}$$

Notice the new variables satisfy symmetry relations and a Pythagorean identity:

$$C_{ij}^t = C_{ji}^t, \quad S_{ij}^t = -S_{ji}^t, \qquad (i,j) \in \mathcal{L},\, t \in \mathcal{T} \tag{19}$$

$$\left(C_{ij}^t\right)^2 + \left(S_{ij}^t\right)^2 = C_{ii}^t \cdot C_{jj}^t, \qquad (i,j) \in \mathcal{L},\, t \in \mathcal{T} \tag{20}$$

Thus the feasible set is now described by the linear and quadratic constraints (5) and (6), together with (10)–(16) and (18)–(20). Note that constraint (13) is readily enforced by the linear constraints $E_i \geq P_{g,i}^t$ and $E_i \geq -P_{g,i}^t$, for $i \in \mathcal{B}$, $t \in \mathcal{T}$.

To obtain a bona fide quadratic program, we must produce a quadratic objective. Under the change of variables, the voltage deviation term (1) becomes

$$\sum_{t\in\mathcal{T}} \sum_{i\in\mathcal{B}} \left(\sqrt{C_{ii}^t} - 1\right)^2. \tag{21}$$

which is clearly not quadratic in the problem variables.

Our main insight here is that the voltage magnitudes are restricted to a small interval around 1 p.u., so we can leverage a Taylor expansion to recover a convex objective without sacrificing much accuracy. Concretely, the second-order Taylor polynomial approximating $f(x) = (\sqrt{x} - 1)^2$ around $x = 1$ is $q(x) = \frac{1}{4}(x-1)^2$, and Taylor's theorem guarantees that the residual in $[1 - \epsilon_-, 1 + \epsilon_+]$ is bounded by $\frac{3}{4!(1-\epsilon_-)^{\frac{5}{2}}} \max\{\epsilon_-, \epsilon_+\}^3$.

In the real-world power systems considered in this work, voltage magnitudes are restricted within 5% of the reference value, so $\epsilon_- = 0.0975$ and $\epsilon_+ = 0.1025$, and the maximum residual is less than 1.74×10^{-4}. Thus we define the voltage deviation term in the new variables as (22). The second-order Taylor approximation $q(x)$ of $f(x) = (\sqrt{x} - 1)^2$ around $x = 1$ and $f(x)$ in a typical interval limiting voltage magnitude deviations of 0.05 p.u. is compared in Fig. 1. The maximum absolute error is 1.27×10^{-4} and the root-mean-square error is 4.73×10^{-5}.

$$C_{V,CP} = \frac{1}{4} \sum_{t\in\mathcal{T}} \sum_{i\in\mathcal{B}} \left(C_{ii}^t - 1\right)^2 \tag{22}$$

Together with (2) and (3), this approximation yields a (non-convex) quadratically constrained quadratic program (QCQP) program in the real variables C, S, E, P_g, P_d, for any given s:

$$\begin{aligned} \text{minimize} \;\; & \alpha C_{V,CP} + \beta C_P + \gamma C_B \\ \text{s.t.} \;\; & (5),\; (6),\; (10) - (16),\; (18) - (20). \end{aligned} \tag{23}$$

This QCQP can be solved with sequential quadratic programming (SQP) techniques.

Since the quadratic equalities (20) describe nonconvex sets, we take a cue from [9] to obtain a convex relaxation using second-order cone programming (SOCP) constraints;

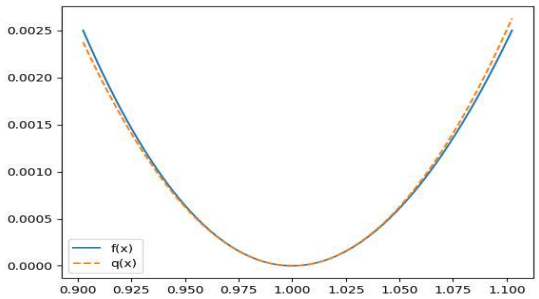


Fig. 1 The second-order Taylor approximation $q(x)$ of $f(x) = (\sqrt{x}-1)^2$ around $x = 1$ in a typical interval limiting voltage magnitude deviations of 0.05 p.u. The maximum absolute error is 1.27×10^{-4} and the root-mean-square error is 4.73×10^{-5}.

in particular, we relax (20) as:

$$\left(C_{ij}^t\right)^2 + \left(S_{ij}^t\right)^2 \leq C_{ii}^t \cdot C_{jj}^t; \qquad (i,j) \in \mathcal{L},\, t \in \mathcal{T} \tag{24}$$

Then (24) can be rewritten as

$$\left(C_{ij}^t\right)^2 + \left(S_{ij}^t\right)^2 + \left(\frac{C_{ii}^t - C_{jj}^t}{2}\right)^2 \leq \left(\frac{C_{ii}^t + C_{jj}^t}{2}\right)^2$$

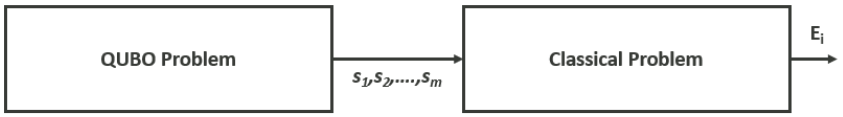
which is nothing more than a rotated cone in $\mathbb{R}^4$. Note this SOCP constraint defines the convex hull of (20).

Combining the SOCP constraint (24) with our quadratic objective yields a disciplined convex program in the real variables C, S, E, P_g, P_d, for any given s:

$$\begin{aligned} \text{minimize} \;\; & \alpha C_{V,CP} + \beta C_P + \gamma C_B \\ \text{s.t.} \;\; & (5),\ (6),\ (10)-(16),\ (18)-(19),\ (24). \end{aligned} \tag{25}$$

3 Two-stage solver: first place, then size

The ESSDP is a MIP because the ESS placement variables s_i are binary. Its coupling of binary decision variables to continuous parameters, together with its nonlinear constraints, is in large part responsible for the complexity of the ESSDP. We propose a two-stage heuristic that decomposes the ESSDP into a binary siting problem followed by a continuous (convex) sizing problem. Motivated by earlier developments introduced in [27], our workflow leverages the best of both quantum and classical computers: it uses a quantum processor to sieve the exponentially large solution space of binary decision variables into a manageable subset of high quality candidate siting vectors, and then hands off a fixed number of them to a fast convex solver running on classical hardware. Figure 2 illustrates our decomposition.



There will be multiple candidate location sets (multiple sets of s_i). Each s_m will have N number of ESS at i^{th} locations. The other M-N locations of each will have zeros. E_i will have the optimal size of N ESS.

Fig. 2 The solution approach to solve the optimal location and size of the ESS.

3.1 Quantum sieve

In the first stage of our decomposition, we approximately solve a binary decision problem to determine candidate ESS location vectors; importantly, this siting problem does not explicitly account for voltage deviation or substation power deviation; rather, it focuses on the economic aspect of deployment. We begin with a binary Linear Program (LP) designed to produce high-quality siting candidates. Next we follow some of the co-authors' earlier work in [27, 31] to interpret the LP as a Hamiltonian energy minimization problem, and use a Variational Quantum Algorithm (VQA) to produce the desired candidate vectors by repeatedly sampling the resulting optimized quantum ansatz.

For the siting problem at this stage, we focus on the economic installation cost objective and notice that feasible placement vectors can be filtered by verifying that the maximum installed capacity exceeds the peak power demanded. Much like in Section III.A in [27], we leverage two simple observations to construct an LP designed to produce location vectors resulting in high-quality approximate solutions to the ESSDP MIP.

Observation 1 The cost $C_{B,i}$ of installing an ESS unit at bus $i \in \mathcal{B}$ is monotonically increasing, so $C_{B,i}(\underline{E_i}) \leq C_{B,i}(E_i)$ for every feasible E_i.

This implies $c_{\min}(s) = \sum_i s_i C_{B,i}(\underline{E_i})$ is a lower bound for the cost of installing ESS units at the buses specified by s. Thus we say s is a *solution candidate* if $c_{\min}(s) \leq C_B(E^*, s^*)$, with E^* and s^* denoting the optimal energy storage capacity and ESS location vector for the ESSDP Problem (17); notice that if s is not a solution candidate, it cannot be an optimal ESS placement vector since

$$C_B(E^*, s^*) < c_{\min}(s) \leq \sum_i s_i C_{B,i}(E^*, s). \tag{26}$$

Observation 2 Location vectors satisfying $s^T \overline{E} \geq \sum_{i \in \mathcal{B}} P_{d,i}$, with $P_{d,i} = \max_{t \in \mathcal{T}} P^t_{d,i}$, are feasible.

This follows immediately from the power generation constraints (12)–(14): the ESS units installed must have enough storage capacity to cover peak power demanded across the system.

Combined, the two observations imply that we can identify solution candidates as location vectors with low minimum installation cost $c_{\min}$ whose corresponding maximum storage capacity profile satisfies peak power demanded. In other words, we seek approximate solutions to the following binary LP:

$$\begin{aligned} \text{minimize} \quad & \sum_{i \in \mathcal{B}} s_i C_{B,i}(\underline{E_i}) \\ \text{s.t.} \quad & \sum_{i \in \mathcal{B}} s_i \overline{E_i} \geq \sum_{i \in \mathcal{B}} P_{d,i} \\ & \sum_{i \in \mathcal{B}} s_i \leq N. \end{aligned} \tag{27}$$

In practice, we follow [27] to cast the binary LP (27) as a Hamiltonian energy minimization problem and approximately solve it with a VQA. For starters, we encode Problem (27) as an unconstrained program with objective function R given by a linear combination of $c_{\min}$ and a penalty term that is a function of the constraint violation.

Whereas standard techniques introduce slack variables when converting a problem with inequality constraints into a QUBO, we leverage the method introduced in [31], which obviates the need for slack variables that typically translate into ancilla qubits in quantum implementations. Instead, our method enforces problem constraints through a penalty term. While our VQA may still sample infeasible states, the penalty terms reduce the probability of sampling generator assignments that cannot satisfy the power demand over the course of the optimization.

By replacing decision variables in the expression of $c_{\min}$ with corresponding Pauli operators, we construct a Hamiltonian corresponding to our quadratic objective using standard methods. Then we follow [31] to obtain an operator H_Q on $|\mathcal{B}|$ qubits such that $H_Q \left|s\right\rangle = R(s) \left|s\right\rangle$, whose eigenvalues can be *lazily* computed on a classical device during the hybrid execution loop upon evaluating constraint violations associated with sampled quantum states directly on the classical processor.

Concretely, our VQA solves approximately the following non-convex optimization problem:

$$\text{minimize}_{\boldsymbol{\theta}} \left\langle \psi(\boldsymbol{\theta}) \right| H_Q \left| \psi(\boldsymbol{\theta}) \right\rangle \tag{28}$$

with $|\psi(\boldsymbol{\theta})\rangle$ denoting the parametrized quantum state defined by our variational circuit of choice.

In this case $|\psi(\boldsymbol{\theta})\rangle$ denotes the layered ansatz illustrated in Figure 1 in [27]. The gate layout is inspired by the quantum alternating operator ansatz structure and it leverages so-called *warm-starting* to define the initial quantum state, which sets the qubit register in a superposition encoding the solution to the semi-definte relaxation of Problem (27). The ansatz layers alternate between an entangling layer, consisting of parametrized ZY gates in the Butterfly Ansatz layout [32], and a simple mixer layer, consisting of parametrized single-qubit rotations. It is worth noting that the all-to-all connectivity of qubits in IonQ systems enables a direct implementation of entangling

gates on non-adjaecent qubit pairs, with no overhead related associated with required swap instructions and qubit rerouting.

Upon convergence of the VQA, we sample the optimized quantum state is sampled to obtain a collection of feasible location vectors with low minimum installation costs– these have the highest chance of being solution candidates. The samples are ranked according to their $c_{\min}$ value and we keep only a fixed number of samples, chosen ahead of time. The remaining subset is returned as the set of solution candidates L^*.

3.2 Classical refinement

With a set C^* of candidate ESS location vectors in hand, we solve the convex sizing Problem (25) a fixed number of times. At this stage we incorporate voltage and substation power, along with total ESS installation cost objectives in the optimization. For each candidate location, the optimal real power requirement is determined for every time interval, and the optimal storage capacity of each ESS results from the peak power requirements.

To conclude, we report the best ESS location vector as

$$\arg\min_{s}\{\alpha C_V(U) + \beta C_S(P) + \gamma C_B(E,s) \mid s \in L^*\}, \tag{29}$$

together with its corresponding U, P, and E values, as determined by the convex solver.

4 Optimization and Result Analysis

To validate the proposed methodology, optimal placement of battery energy storage in standard test cases (IEEE 13- and 33-bus distribution systems) using the proposed quantum-classical solution framework was solved. The QUBO problem corresponding to the test cases was solved using IonQ's Forte quantum computer. In addition, we solved the QUBO problem for Test Case I using IonQ's cloud simulator.

For both cases, the average bus voltage ($\overline{U}$), sub-station voltage, and the average substation power ($\overline{P}$) were considered as 1.0 p.u., 1.0 p.u., and 0.5 MW, respectively. The installation costs were assumed to be identical across all possible locations, and the cost function C_i is considered$\{a, b, c\} = \{0.01, 460, 1\}$ for a quadratic function, $C_i = ax^2 + bx + c$ [33] apart from the sub-station and substation cost is kept higher. The 24-hour load profile is taken from the EPRI US load factors: {0.677, 0.6256, 0.6087, 0.5833, 0.58028, 0.6025, 0.657, 0.7477, 0.832, 0.88, 0.94, 0.989, 0.985, 0.98, 0.9898, 0.999, 1, 0.958, 0.936, 0.913, 0.876, 0.876, 0.828, 0.756} [34].

4.1 Test case I: 12-Bus Distribution System

The 12-bus distribution system is derived from the IEEE 13-bus distribution system. For clarity in presentation, we removed bus-680 and relabeled the remaining buses as in Section 2. Fig. 3 illustrates the one-line diagram of Test System I. A single-phase equivalent representation of the multi-phase IEEE 13 bus system was considered for the evaluation of the solution methods proposed in this paper. The system's data are

taken from [35]. In the modified system, the switch between bus-671 and bus-692 is assumed closed. All network parameters were converted into per-unit (p.u.) system for consistency. The on-load tap changer (OLTC) transformer located between bus-650 and bus-632 was modeled with a fixed tap position of 0 throughout the study.

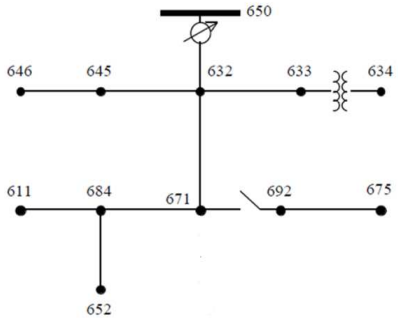


Fig. 3 One-line diagram of the modified 12-Bus Distribution System (Test System I).

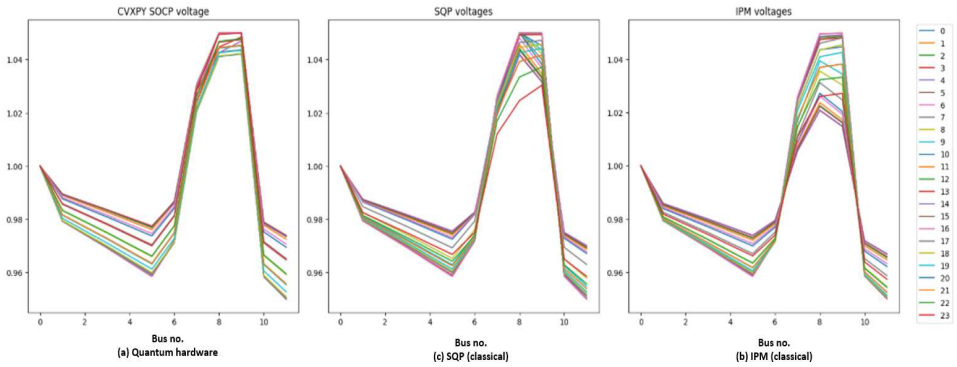
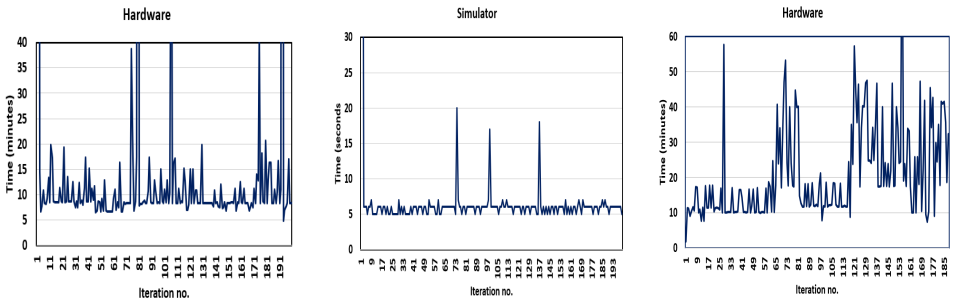


Fig. 4 Voltage profile comparison of 12-bus distribution system (Test System I). (a) Quantum computer, (b) SQP (classical), and (c) IPM (classical). Shown are voltage for each of the 12 underlying buses, indicating how the voltages change a 24 hours time period. The figures show good alignment between the quantum prediction shown in (a) and the two baselines shown in (b) and (c), namely sequential quadratic programming (SQP) and interior point method (IPM).

Fig. 4 illustrates voltage profiles obtained using our two-stage heuristic. To compute these, we first ran the VQA described in Section 3 to solve an appropriate QUBO program using IonQ Forte. For comparison, we also solved the QUBO using IonQ's cloud simulator. The quantum backends were used in conjunction with Scipy's implementation of the Constrained Optimization by Linear Approximation (COBYLA) algorithm [36] to tune our variational quantum ansatz, using 512 shots to sample the parametrized quantum state at each COBYLA iteration. We used Scipy's default stopping criterion to halt the optimization, and in each case we tuned the hyper-parameter



(a) (b) (c)

Fig. 5 Time required for each iteration for (a) quantum hardware and (b) quantum simulator for test system I, and (c) quantum hardware for test system II.

λ experimentally, and initialized circuit parameters as $\boldsymbol{\theta} = 0$. With each set of optimized parameters $\boldsymbol{\theta}^*$ in hand, we sampled the quantum state $|\psi(\boldsymbol{\theta}^*)\rangle$ resulting from the VQA using $5,000$ shots. We filtered out the infeasible samples and sorted the feasible assignment vectors by minimum installation cost. We then solved at most 25 residual continuous problems corresponding to the top candidate location vectors and chose the siting and sizing that yielded the best overall objective value.

For comparison and validation of our convex relaxation, we fixed the best ESS location vector and solved the residual ESSDP (17) using MATLAB's interior-point method (IPM) solver, the QCQP formulation (23) using MATLAB's SQP routine, and our convex relaxation (25) using CVXPY's ECOS solver.

The optimization results obtained from IonQ quantum simulator and IonQ Forte quantum computer are compared. The two backends sampled the best overall configuration, and showed similar results. 200 iterations were perfomred on IonQ's cloud simulator and IonQ's Forte QPU. The times taken for each iteration on IonQ Forte and IonQ's cloud simulator are illustrated in Fig. 5 (a) and (b). Excluding outliers, the average time for each iteration on the cloud simulator was 6.8 seconds and it was 8-9 minutes on IonQ Forte. It can be observed that The simulator maintains a very tight "floor" near 5–6 seconds, whereas the hardware baseline is much "noisier," fluctuating constantly between 7 and 15 minutes even without the major spikes. In Fig. 5 (b), there is a significant spike at the very first iteration (approaching 30 seconds). This is common in simulators due to initial memory allocation or circuit compilation. The spikes in the hardware graph (reaching 40 minutes), Fig. 5 (a), likely represent overhead beyond pure computation, such as cloud queuing, calibration cycles, or network latency. So, it can be opined that there is a massive disparity in execution speed. If we take the average hardware time as 8.5 minutes (510 seconds) and the simulator at 6.8 seconds, the simulator is approximately 75 times faster than the physical hardware for these iterations. This is because, physical quantum hardware requires complex state preparation, laser cooling, and gate operations that are physically performed on ions. Additionally, cloud-access hardware often involves job queuing that can add significantly to the "iteration time" compared to a classical simulator that mimics the math of the circuit locally or on optimized classical clusters. Given the

Table 1 ESS capacity (kWh) and location for 12-bus distribution system for IonQ Forte quantum computer, IonQ quantum simulator, classical-SQP, and classical-IPM.

In. no.	ESS location (Bus no.)	Quantum computer	Quantum simulator	SQP (classical)	IPM (classical)
1	671	128	128	128	125.2
2	652	576.2	576.2	715.3	588.4
3	611	1055	1055	1126.1	1123.1

two-order-of-magnitude speed advantage and higher stability of the cloud simulator, it is the primary choice for iterative development and hyperparameter tuning, while IonQ Forte is reserved strictly for final-stage validation.

The optimization profile for Test System I is illustrated in Fig. 6. The optimization profile of the VQA for the QUBO problem on IonQ Forte is initialized at $\theta = 0$, the COBYLA routine exhibits a rapid initial convergence, successfully navigating the high-dimensional cost landscape to transition from a penalty-dominated state (≈ 5000) to a feasible region within the first 60 iterations. While the optimizer reaches a minimum objective value of 2725.175, the trajectory is characterized by significant stochastic volatility and high-frequency oscillations thereafter. These fluctuations, particularly the pronounced spikes observed near iterations 90 and 100, are likely attributable to the interplay between the hardware's physical gate noise and the statistical shot noise inherent to the 495-shot sampling limit. Such behavior suggests that while the IonQ Forte hardware is capable of identifying deep local minima for this test system, the noise floor prevents the derivative-free optimizer from reaching a stable convergence plateau, highlighting the trade-off between execution overhead and solution stability in near-term quantum devices.

The optimized ESS locations computed by both IonQ Forte and IonQ's cloud simulator were bus 7, 9, and 10. The maximum relative error when comparing the voltage profiles computed by our SOCP solver, given ESS placements at bus 7, 9, and 10, against the SQP and IPM solvers is 2.434% and 3.335%, respectively. From the results, the performance of the IonQ quantum simulator and IonQ Forte quantum computer are similar with maximum error with respect to the classical solution and is well below the accepted thresholds. The negligible relative error (¡3.34%) in the resulting voltage profiles validates the VQA's ability to maintain high solution fidelity on physical hardware, providing a foundation for applying these quantum heuristics to larger-scale distribution networks where classical exact solvers face scaling limitations.

The optimized capacity of the recommended ESS in kWh is reported in Table 1. The comparison with classical SQP and IPM solvers serves two primary purposes: validation and performance benchmarking. First, as a feasibility study, matching the classical solvers' identified bus locations (7, 9, and 10) confirms that the quantum algorithm can accurately resolve the combinatorial complexity of the placement problem. Second, as a performance bonus, the quantum results in Table 1 demonstrate superior lower ESS capacity values compared to the classical baselines. Specifically,

for Bus 652 and 611, the IonQ Forte identified feasible ESS capacities that were significantly lower than those found by SQP and IPM (e.g., 576.2 kWh vs. 715.3 kWh for Bus 652). Since the resulting voltage profile errors remained within a negligible range, these results suggest that the quantum-classical hybrid approach successfully explored more efficient regions of the solution space, yielding more cost-effective infrastructure requirements than traditional gradient-based classical methods.

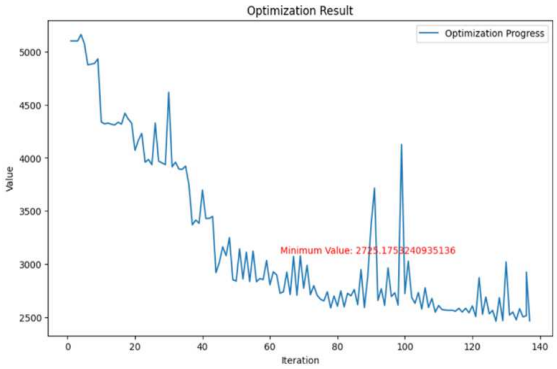


Fig. 6 Convergence of the VQA described in Section 3 solving the 12-variable QUBO (27) corresponding to Test System I on IonQ Forte. We used Scipy's implementation of the COBYLA routine to train our variational ansatz with initial parameters $\theta = 0$. Each iteration used 495 shots and the constraint penalty hyperparameter was fixed at $\lambda = 5,000$.

4.2 Test Case II: 32-Bus Distribution System

The methods is tested with 32-bus distribution system, which is a modified version of IEEE-33 bus distribution system. The system data are taken from [37]. The system comprises 31 branches and its voltage rating is 12.66 kV. The total system load is 3.715 MW and 2.8 Mvar. The system is illustrated in Fig. 7.

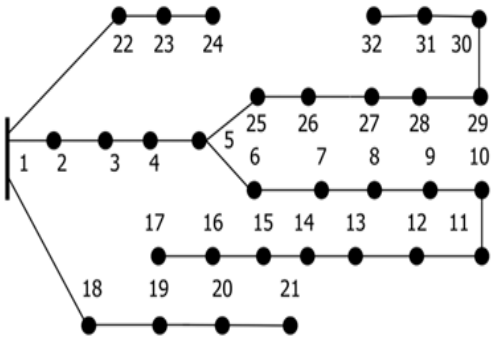


Fig. 7 One line diagram of the modified 32-bus distribution system (Test System II).

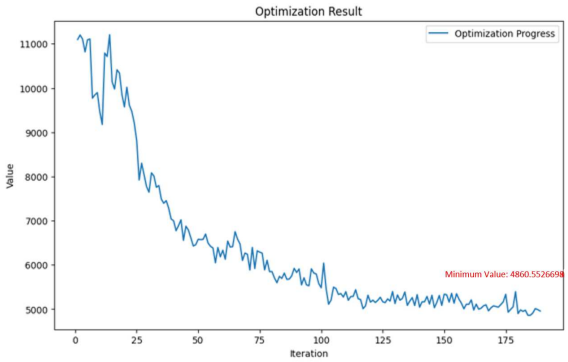


Fig. 8 Convergence of the VQA described in Section 3 solving the 32-variable QUBO (27) corresponding to Test System I on IonQ Forte. We used Scipy's implementation of the COBYLA routine to train our variational ansatz with initial parameters $\theta = 0$. Each iteration used 495 shots and the constraint penalty hyperparameter was fixed at $\lambda = 10,000$.

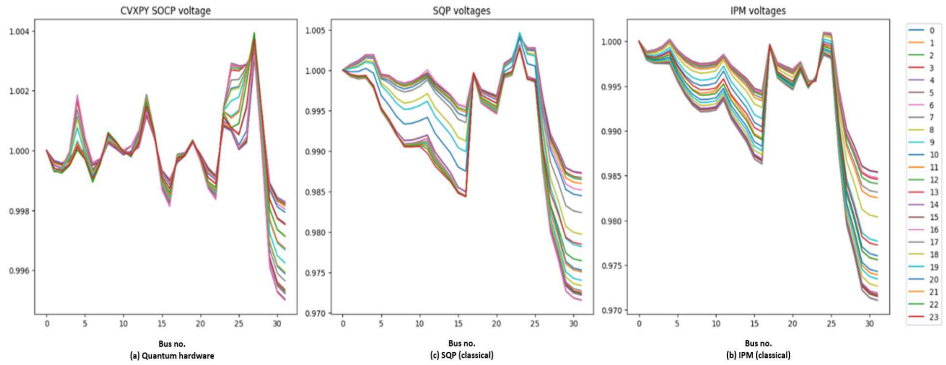


Fig. 9 Voltage profile comparison of 32-bus distribution system (Test System II). (a) Quantum computer, (b) SQP (classical), and (c) IPM (classical). Shown are voltage for each of the 32 underlying buses, indicating how the voltages change a 24 hours time period. The figures show good alignment between the quantum prediction shown in (a) and the two baselines shown in (b) and (c), namely sequential quadratic programming (SQP) and interior point method (IPM). The maximum relative error with respect to as is determined as 2.417% and 2.531%, respectively.

The ESS siting and sizing optimization problem is solved through the IonQ Forte quantum computer. The resulting optimization profile is illustrated in Fig. 8. The optimization trajectory for the 32-variable QUBO on IonQ Forte, representing a more complex scaling of the ESS placement problem, is depicted in Fig. 8. Initialized at $\theta = 0$, the VQA exhibits an aggressive descent during the first 100 iterations, effectively driving the cost function from an initially infeasible state (≥ 11000) to below the constraint penalty threshold of $\lambda = 1000$. The optimizer reaches a minimum value of 4860.55, demonstrating the hardware's capability to navigate a significantly larger Hilbert space compared to the 12-variable case. Similar to the smaller test system,

Table 2 ESS capacity (kWh) and location for 32-bus distribution system for IonQ Forte quantum computer, classical-SQP, and classical-IPM.

In. no.	ESS location (Bus no.)	Quantum computer	SQP (classical)	IPM (classical)
1	9	314.64	349.33	350.03
2	14	423.34	418.48	419.51
3	20	203.94	481.98	480.68
4	24	745.15	903.55	902.32
5	25	654.936	774.63	773.13
6	28	873.99	796.98	798.13

the profile displays persistent high-frequency oscillations in the late-stage iterations (125–200). These fluctuations are characteristic of the interplay between physical gate noise on the IonQ Forte and the statistical variance resulting from the 495-shot sampling limit. Despite these stochastic effects, the resulting ESS configuration achieved a high level of physical accuracy, with maximum relative voltage errors of only 2.417% and 2.531% compared to classical SQP and IPM solvers, respectively. This confirms that the VQA remains robust and competitive with classical benchmarks even as the problem dimensionality increases.

The time taken for each iteration for IonQ quantum computer is illustrated in Fig. 5 (c). Compared to the 12-variable case, the baseline iteration time increased to approximately 12–15 minutes, reflecting the higher compilation and execution overhead associated with increased circuit depth. Notably, the profile exhibits significant temporal volatility, with frequent spikes exceeding 40 minutes and peaking at 60 minutes per iteration. These delays are primarily attributed to cloud-based queuing latencies and necessary hardware recalibration intervals on the IonQ Forte platform. The substantial increase in total wall-clock time for the 32-variable system underscores the necessity of the hybrid development workflow: utilizing the cloud simulator for iterative algorithmic tuning and reserving the physical hardware for final-stage validation where physical noise characteristics are the primary focus.

The comparative results for the 32-bus system, summarized in Table 2, further emphasize the performance benefits of the quantum-classical hybrid approach. While the classical SQP and IPM solvers provided valid baselines, the IonQ Forte identified superior objective function values (lower ESS capacities) across the majority of the siting locations. A significant result is observed at Bus 20, where the quantum computer determined an optimal capacity of 203.94 kWh—representing a 57.6% reduction compared to the 481.98 kWh required by the SQP solver. Similarly, at Bus 24 and 25, the quantum-derived capacities were significantly more efficient than the classical benchmarks. Given that these solutions maintain a voltage profile error of less than 2.54% (as shown in Fig. 9), these findings demonstrate that for higher-dimensional problems, the quantum heuristic can navigate the non-convex solution space more effectively than traditional gradient-based methods, discovering deeper minima that offer substantial infrastructure cost savings.

4.3 Advantage of the Proposed Method

A primary methodological advantage is observed when decoupling the discrete siting search from the continuous sizing refinement. Traditional classical methods, particularly monolithic mixed-integer programming (MIP), can encounter scalability bottlenecks and sensitivity to relaxation gaps when handling high-fidelity network constraints. As illustrated in Fig. 10, a standard monolithic MIP solver identifies a solution that distributes ESS capacity across nearly all 12 buses. While this 'dense' configuration may appear mathematically optimal for minimizing total kWh and might be beneficial for the voltage and electrical perspective, it is practically unfeasible due to the high fixed capital expenditures associated with multiple site interconnections. Our quantum-classical hybrid approach (Table 1) identifies a sparse solution (Buses 7, 9, and 10) that concentrates the required capacity. This demonstrates that the quantum heuristic, when mapped via QUBO, naturally gravitates toward more practical, sparse infrastructure configurations that avoid the 'dimensionality curse' and the impractical siting outcomes inherent to monolithic classical optimization.

While a cardinality constraint could theoretically be introduced into a classical monolithic MIP to limit ESS siting, this approach introduces significant computational overhead and numerical instability due to the expansion of the branch-and-bound search tree. Furthermore, monolithic MIP solvers often rely on linearizations or relaxations of the power flow equations to maintain tractability. By contrast, the decoupled quantum-classical approach uses the IonQ Forte to navigate the combinatorial siting space (the 'where') and a high-fidelity SOCP solver for sizing (the 'how much'). This decoupling ensures that the physical network constraints are never relaxed, providing a more robust and scalable framework for large-scale distribution networks where monolithic solvers typically encounter prohibitive relaxation gaps.

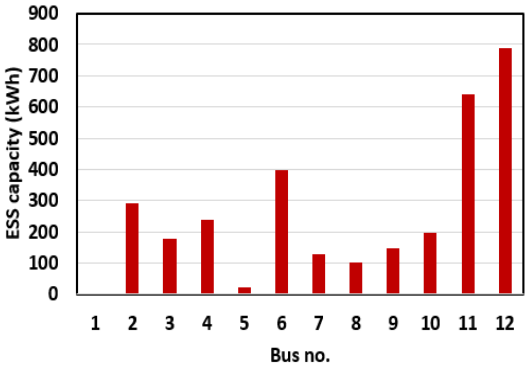


Fig. 10 Capacity of ESS when using monolithic MIP for 12-bus distribution system (Test System I).

The proposed hybrid framework utilizes the quantum hardware as a stochastic sieve to sample a diverse portfolio of high-quality candidate-site sets. This sampling capability allows planners to explore alternative configurations that may offer superior practical or unmodeled reliability benefits. The subsequent classical refinement

stage (SOCP) then acts as a physical anchor, ensuring that the quantum-derived configurations adhere to strict grid-standard voltage requirements. By benchmarking these results against IPM, we demonstrate that the quantum-discovered configurations are not only mathematically superior in terms of objective value (lower capacity) but are also electrically robust, maintaining physical fidelity within industry-accepted thresholds.

5 Toward quantum scalability

This work utilizes a Variational Quantum Algorithm (VQA) as a near-term heuristic for energy storage system (ESS) siting. However, the long iteration times on current hardware and the susceptibility of VQAs to barren plateaus necessitate a shift in algorithmic strategy for industrial-scale distribution networks. To address the exponentially growing combinatorial search space of larger systems, there are several options worth pursuing.

A promising pathway to scalability involves transitioning from heuristic sampling to Quantum Phase Estimation (QPE). By encoding the siting problem (Eq. (27)) into a Hamiltonian, QPE offers a non-heuristic mechanism to find the ground state energy (the optimal siting) with predictable complexity. A critical hurdle for QPE in realistic power systems is the initial state preparation. QPE requires an initial state with a non-negligible overlap with the ground state to avoid exponential repetitions. If the overlap condition is met, QPE provides a provable mechanism to explore the siting landscape more efficiently than classical brute force, establishing a formal limit for quantum advantage in grid planning.

To bypass the barren plateaus inherent in VQA, Quantum Imaginary Time Evolution (QITE) represents a robust alternative. QITE evolves a state toward the ground state of the siting Hamiltonian by simulating non-unitary imaginary time evolution. QITE is physically inspired, generally more reliable than VQA in avoiding local minima in complex energy landscapes, and less sensitive to initial state overlap than QPE. However, it requires significant measurement overhead and circuit depth on gate-based hardware, which current NISQ devices are not yet equipped to handle at scale.

The main advantage of our current work lies in the two-stage decomposition. By isolating the exponential complexity of siting (Stage I) from the polynomial efficiency of convex sizing (Stage II), the framework remains quantum-ready. As hardware and state-preparation algorithms evolve, the quantum sieve can be upgraded from VQA to scalable quantum algorithms, such as variants of QPE or QITE, without altering the rigorous physical refinement of the classical stage.

6 Conclusion and Future Work

In this paper, a novel two-stage ESS planning framework is introduce and designed to decouple binary siting decisions from continuous sizing and operational problems. By reformulating the siting task as a Quadratic Unconstrained Binary Optimization

(QUBO) problem, a hybrid quantum-classical workflow is successfully implemented using IonQ Forte hardware. This approach ensures that the discrete combinatorial search is performed on quantum hardware while the continuous dispatch is maintained within a physically rigorous convex optimization model. The experimental results validate the methodological integration of quantum backends into grid planning workflows. The quantum hardware experiments produced distinct candidate-site sets compared to purely classical approaches, highlighting the potential of quantum sampling to broaden the solution landscape for ESS planning.

Future research will transition this framework from a proof-of-concept to a scalable industrial tool by addressing the fundamental hurdles of state preparation and algorithmic efficiency. We will explore the transition from Variational Quantum Algorithms (VQA) to Quantum Phase Estimation (QPE). While QPE offers a provable scaling path, future studies must specifically address the initial state-preparation problem to ensure sufficient ground-state overlap in realistic grid cost landscapes. We intend to investigate Quantum Imaginary Time Evolution (QITE) as a means to bypass the barren plateaus often encountered in VQA, providing a more stable convergence path for high-dimensional siting problems.

Real-world utility deployments involve higher-order interactions between ESS units, such as shared regional infrastructure costs. We will extend our current objective function (Eq. (27)) to include these non-linear interdependencies, leveraging the high connectivity of gate-based quantum systems to map these Higher-Order Binary Optimization (HOBO) problems.

It should be noted that the current formulation in Eq. (27) assumes that installation costs are additive and independent across buses. While this serves as a baseline for distributed storage, a more comprehensive planning scope for large-scale utility deployment would necessitate the inclusion of higher-order interaction terms to account for shared infrastructure or regional constraints. In a realistic utility scenario, the cost of installing an ESS at bus i may be influenced by the existence of a unit at bus j, requiring a move from linear-binary objectives to Higher-Order Binary Optimization (HOBO). It is important to note that the transition to a HOBO model is a matter of problem definition rather than a limitation of the hybrid solver. While higher-order terms increase the complexity for both classical and quantum methods, the proposed QUBO/Hamiltonian mapping is natively capable of incorporating these interactions through the use of ancilla qubits or higher-order term reductions. Future expansions of the problem scope to include these interdependencies would benefit from the high connectivity of hardware like the IonQ Forte, which can map complex, non-local cost interactions with minimal gate overhead compared to standard grid-based topologies.

The framework will be extended to include system reliability analysis, ensuring that the diverse solution sets provided by the quantum sieve meet stringent operational resilience standards.

Acknowledgements. Authors would like to thank Rima Oueid and Alireza Ghassemian for overseeing the project developments and providing guidance.

Funding Declarations

This research used resources of the Oak Ridge Leadership Computing Facility, which is a DOE Office of Science User Facility supported under Contract DE-AC05-00OR22725. This work was supported by the U.S. Department of Energy's Grid Modernization Initiative (GMI) Grid Research, Integration, and Deployment for Quantum (GRID-Q) project. This manuscript has been authored by UT-Battelle, LLC under Contract No. DE-AC05-00OR22725 with the U.S. Department of Energy. The United States Government retains and the publisher, by accepting the article for publication, acknowledges that the United States Government retains a non-exclusive, paid-up, irrevocable, world-wide license to publish or reproduce the published form of this manuscript, or allow others to do so, for United States Government purposes. The Department of Energy will provide public access to these results of federally sponsored research in accordance with the DOE Public Access Plan (https://www.energy.gov/doe-public-access-plan).

Author Contributions

Md Shamim Hasan and Willie Aboumrad conceived the study, developed the mathematical models and code, and wrote the initial manuscript. P.R.V. Marthi, E. Epifanovsky, G. Siopsis, M. Roetteler, and S. Debnath contributed to the conceptual and mathematical design, assisted with coding, and participated in the writing and editorial review of the manuscript.

References

[1] Wichitkrailat, K., Premrudeepreechacharn, S., Siritaratiwat, A. & Khunkitti, S. Optimal sizing and locations of multiple besss in distribution systems using crayfish optimization algorithm. *IEEE Access* **12**, 94733–94752 (2024).

[2] An, J. & Hong, T. Multi-objective optimization for optimal placement of shared battery energy storage systems in urban energy communities. *Sustainable Cities and Society* **120**, 106178 (2025).

[3] Li, B. *et al.* Review on photovoltaic with battery energy storage system for power supply to buildings: Challenges and opportunities. *Journal of Energy Storage* **61**, 106763 (2023).

[4] Jaradat, T. & Khatib, T. Optimal sizing of battery energy storage system in electrical power distribution network. *Energy Exploration & Exploitation* **43**, 909–931 (2025).

[5] Stecca, M., Elizondo, L. R., Soeiro, T. B., Bauer, P. & Palensky, P. A comprehensive review of the integration of battery energy storage systems into distribution networks. *IEEE Open Journal of the Industrial Electronics Society* **1**, 46–65 (2020).

[6] Stecca, M., Elizondo, L. R., Soeiro, T. B. & Bauer, P. *Energy storage sizing and location in distribution networks considering overall grid performance*, 1–5 (2020).

[7] Boonluk, P., Siritaratiwat, A., Fuangfoo, P. & Khunkitti, S. Optimal siting and sizing of battery energy storage systems for distribution network of distribution system operators. *Batteries* **6**, 56 (2020).

[8] Gupta, R. & Sossan, F. Optimal sizing and siting of energy storage systems considering curtailable photovoltaic generation in power distribution networks. *Applied Energy* **339**, 120955 (2023).

[9] Kocuk, B., Dey, S. S. & Sun, X. A. Strong SOCP relaxations for the optimal power flow problem. *Operations Research* **64**, 1177–1196 (2016).

[10] Glover, F., Kochenberger, G. & Du, Y. A tutorial on formulating and using qubo models. *arXiv preprint arXiv:1811.11538* (2018).

[11] Lucas, A. Ising formulations of many NP problems. *Frontiers in physics* **2**, 5 (2014).

[12] Morstyn, T. Annealing-based quantum computing for combinatorial optimal power flow. *IEEE Transactions on Smart Grid* **14**, 1093–1102 (2023).

[13] Colucci, G., Linde, S. v. d. & Phillipson, F. Power network optimization: A quantum approach. *IEEE Access* **11**, 98926–98938 (2023).

[14] Kaseb, Z., Möller, M., Vergara, P. P. & Palensky, P. Power flow analysis using quantum and digital annealers: a discrete combinatorial optimization approach. *Scientific Reports* **14**, 23216 (2024).

[15] Chen, Y. & Vu, T. L. A review of quantum computing technologies in power system optimization (2025).

[16] Hossain, M. B., Islam, M. R., Muttaqi, K. M., Sutanto, D. & Agalgaonkar, A. P. Advancement of fuel cells and electrolyzers technologies and their applications to renewable-rich power grids. *Journal of Energy Storage* **62**, 106842 (2023).

[17] Nazaripouya, H., Wang, Y., Chu, P., Pota, H. R. & Gadh, R. *Optimal sizing and placement of battery energy storage in distribution system based on solar size for voltage regulation*, 1–5 (IEEE, 2015).

[18] Farsadi, M., Sattarpour, T. & Nejadi, A. Y. *Optimal placement and operation of bess in a distribution network considering the net present value of energy losses cost*, 434–439 (IEEE, 2015).

[19] Zolfaghari, M., Ghaffarzadeh, N. & Ardakani, A. J. Optimal sizing of battery energy storage systems in off-grid micro grids using convex optimization. *Journal of Energy Storage* **23**, 44–56 (2019).

[20] Yuan, Z., Wang, W., Wang, H. & Yildizbasi, A. A new methodology for optimal location and sizing of battery energy storage system in distribution networks for loss reduction. *Journal of Energy Storage* **29**, 101368 (2020).

[21] Tang, X., Deng, K., Wu, Q. & Feng, Y. Optimal location and capacity of the distributed energy storage system in a distribution network. *IEEE Access* **8**, 15576–15585 (2020).

[22] Khaki, B. Joint sizing and placement of battery energy storage systems and wind turbines considering reactive power support of the system. *Journal of Energy Storage* **35**, 102264 (2021).

[23] Alhammad, H. I., Khan, K. A., Alismail, F. & Khalid, M. *Capacity optimization and optimal placement of battery energy storage system for solar pv integrated power network*, 847–852 (IEEE, 2021).

[24] Optimization, G. 4 key advantages of mov's heuristics. *Mathematical Optimization vs. Heuristics* 1–7 (2022).

[25] Wang, J. *et al. Multi-objective optimal allocation of battery energy 3storage systems in distribution network with high penetration of renewable energy*, 1281–1287 (2025).

[26] Yang, M., Chen, C., Que, B., Zhou, Z. & Yang, Q. *Optimal placement and configuration of hybrid energy storage system in power distribution networks with distributed photovoltaic sources*, 1–6 (IEEE, 2018).

[27] Aboumrad, W., Marthi, P. R. V., Debnath, S., Roetteler, M. & Epifanovsky, E. *A New Hybrid Quantum-Classical Algorithm for Solving the Unit Commitment Problem* , 1905–1915 (IEEE Computer Society, Los Alamitos, CA, USA, 2025). URL https://doi.ieeecomputersociety.org/10.1109/QCE65121.2025.00208.

[28] Ling, J., Zhang, Q., Geng, G. & Jiang, Q. Hybrid quantum annealing decomposition framework for unit commitment. *Electric Power Systems Research* **238**, 111121 (2025).

[29] Quinton, F. A., Myhr, P. A. S., Barani, M., Crespo del Granado, P. & Zhang, H. Quantum annealing applications, challenges and limitations for optimisation problems compared to classical solvers. *Scientific Reports* **15**, 12733 (2025).

[30] Jabr, R. Radial distribution load flow using conic programming. *IEEE Transactions on Power Systems* **21**, 1458–1459 (2006).

[31] Kaushik, A. *et al.* Quantum computing for optimizing aircraft loading (2025). URL https://arxiv.org/abs/2504.01567. arXiv:2504.01567.

[32] Cherrat, E. A. *et al.* Quantum Vision Transformers. *Quantum* **8**, 1265 (2024). URL https://doi.org/10.22331/q-2024-02-22-1265.

[33] Das, C. K., Bass, O., Kothapalli, G., Mahmoud, T. S. & Habibi, D. Optimal placement of distributed energy storage systems in distribution networks using artificial bee colony algorithm. *Applied energy* **232**, 212–228 (2018).

[34] Montenegro, D. & Dugan, R. *OpenDSS and OpenDSS-PM open source libraries for NI LabVIEW*, 1–5 (IEEE, 2017).

[35] Schneider, K. P. *et al.* Analytic considerations and design basis for the ieee distribution test feeders. *IEEE Transactions on Power Systems* **33**, 3181–3188 (2018).

[36] Powell, M. J. in *A direct search optimization method that models the objective and constraint functions by linear interpolation* 51–67 (Springer, 1994).

[37] Hasan, M. S., Chowdhury, M. M.-U.-T., Biswas, B. D. & Kamalasadan, S. Semi-definite programming based scalable and accurate optimal power flow models for radial distribution networks. *IEEE Transactions on Industry Applications* **60**, 1463–1475 (2024).